2.5D downward continuation using data mapping theory, Part II: Models and analysis

Steven Sheaffer & Norman Bleistein
Center for Wave Phenomena

ABSTRACT

Data mapping is a procedure for transforming seismic or acoustic data collected with one set of source/receiver locations and wavespeed model, to data equivalent to that collected in a different source/receiver configuration and wavespeed model. A major application of this general process is downward continuation of the wavefield, or wave-equation datuming.

In the 1998 Project Review, a paper by the authors (Sheaffer & Bleistein, 1998) presented a method for performing downward continuation of receivers given a common source gather, and, of sources given a common receiver gather, based on the data mapping theory of Bleistein & Jaramillo (1997). Unlike many previous implementations of the downward continuation process, this procedure yields the correct dynamic result in heterogeneous media, at least in a model-consistent sense. The shot gather and receiver gather geometries permit some simplification to the general data mapping procedure, allowing the derivation of more tractable expressions for datuming. The referenced paper contains this derivation, plus a more explicit methodology for applying the results in constant wavespeed media.

In this paper, some features and limitations of this method are discussed, using examples based largely on the illustrative case of constant wavespeed. Included are a series of synthetic problems, for the purpose of demonstrating amplitude preservation in the process, a discussion of limitations and requirements of the process, consistent with the use of the stationary phase method in the derivations and interpretation, and finally, a comparison between this method and a more commonly applied Kirchhoff datuming method.

Key words: data mapping, downward continuation, wave-equation datuming

Introduction

The data mapping platform of Bleistein & Jaramillo (1997) is a mathematical procedure for transforming data collected in one source and receiver configuration and earth model, to equivalent data collected in a different source and receiver configuration and earth model. In Sheaffer & Bleistein (1998), hereafter referred to as SB98, the general data mapping problem is specialized to the case of downward continuation of the wavefield. In the case of the downward continuation of receivers, where the input data is a common shot gather, the general problem permits some simplifications, and allows the derivation of specific expressions for performing the process in heterogeneous media. The case of downward continuation of sources, where the input data is a common receiver gather, yields an analogous result. Thus, an entire data set, both shots and receivers, can be downward continued via this process. Additionally, the method makes no reference to the shape of the recording surface, and is, thus, correct for topographic recording and datuming surfaces.

In SB98, simplifications pertaining to the case of media with constant background wavespeed are applied to the general expressions, producing a more easily implementable procedure, involving only analytic calcula-

tions. Thus, further studies of the method using simple models can be easily performed. Furthermore, many conventional Kirchhoff-style datuming procedures are performed under the assumption of constant wavespeed amplitudes, and thus, direct comparisons of the methods can be made.

This paper presents three discussions concerning this datuming procedure. First, results of downward continuations of synthetic data over single reflectors are discussed, for various combinations of horizontal and irregular recording and reflecting surfaces. Next, the assumptions and limitations inherent in the procedure are discussed, mainly in the context of finite data aperture and the use of the stationary phase method. Finally, then, a direct comparison between this methodology and a more conventional Green's Theorem approach to the problem is presented and discussed.

Correction in Previous Results

Before continuing, please note an error in SB98. In the specialization of the data mapping procedure to constant wavespeed media, the factor $G(\overline{x}_1, \overline{x}_3)$ is defined. This factor contains the derivatives of the recording surface. However, the definition of this factor given in equation (36) of SB98, as well as its derivation in the Appendix of that paper, is incorrect. The Appendix of this paper is a correction of, and therefore replaces, the Appendix of SB98. Thus, the new definition,

$$G\left(\overline{x}_1, \overline{x}_3\right) \;=\; \left| (\overline{x}_3 - z_I) - (\overline{x}_1 - \xi_I)\, \frac{\partial z_I}{\partial \xi_I} \right| \;, \qquad (1)$$

replaces that given in equation (36) of SB98 for receiver continuation, and the analogous expression for source continuation,

$$G\left(\overline{x}_1, \overline{x}_3\right) \;=\; \left| (\overline{x}_3 - z_I) - (\overline{x}_1 - \eta_I)\, \frac{\partial z_I}{\partial \eta_I} \right| \;, \qquad (2)$$

replaces equation (61) of SB98.

Note that the error is only relevant when the recording surface is topographic. The value of G in the case of a horizontal recording surface using the corrected results is equivalent to that stated in the previous paper using the incorrect result for this factor.

Synthetic Models

Computer codes have been developed to perform downward continuation by the process described in SB98, where the assumption of constant wavespeed is made for amplitude determination. This refers to equation (37) in SB98 for receiver continuation given a common source, and equation (60) in SB98 for source continuation. The codes are implemented as part of the Seismic Unix (SU) processing suite, maintained by the Center for Wave Phenomena, at the Colorado School of Mines.

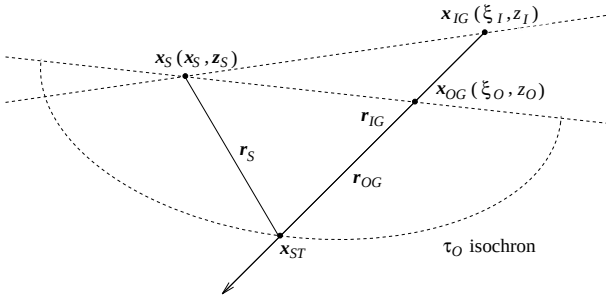

Figure 1. Geometry for receiver continuation in a constant wavespeed medium.

The results of several synthetic data examples will be presented to outline the general features of the output data. Examples from both horizontal and irregular recording and datuming surfaces will be presented. In these models, results of the downward continuation of receivers only for a single fixed source are given, since the continuation of the source is simply the same process under the interchange of source and receiver. Therefore, demonstration of the ability to downward continue receivers shows the validity of the process for source continuation as well.

As is described in SB98, the downward continued field at a given output receiver location and output time is equal to an integration over the data traces, or equivalently, over the input receiver locations on the surface. This integration is, in practice, a sum of component values, each depending on the integration variable. These values are the product of two factors. The first is a weighting factor, which is a function of quantities measured along the raypaths connecting the fixed source and output receiver locations and the location of the input receiver being considered, through a particular stationary point in the subsurface, associated with the chosen output time. The second is the value of the frequency filtered input data from the appropriate input receiver evaluated at a time equivalent to the travel time along one of these raypaths. The stationary points are a result of the use of the method of stationary phase in the derivation, and each component of the integration has a different stationary point.

In a constant wavespeed medium, downward con-

tinuation of receivers is performed using equation (37) of SB98,

$$u_O\left(\xi_O, t_O\right) \approx \frac{1}{\sqrt{2\pi c}} \int d\xi_I \frac{G\left(\overline{x}_1, \overline{x}_3\right)}{r_{IG}} \cdot \frac{\sqrt{r_S + r_{IG}}}{\sqrt{r_S + r_{OG}}\,\sqrt{|r_{IG} - r_{OG}|}} D_f\left(\xi_I, \tau_I\left(\boldsymbol{x}, \xi_I\right)\right).$$

$$D_f\left(\xi_I, t\right) = \frac{1}{2\pi} \int \sqrt{|\omega_I|}\; u_I\left(\xi_I, \omega_I\right) e^{-i\omega_I t + i\pi/4\,\mathrm{sgn}\,(\omega_I)} d\omega_I. \tag{3}$$

This gives the field at a given output receiver location, $\boldsymbol{x}_{OG}(\xi_O)$ and output time, t_O. The geometry for each of the integration components is shown in Figure 1, which is similar to Figure 4 in SB98. Here $\boldsymbol{x}_S$ is the fixed source location, $\boldsymbol{x}_{IG}$ is one of the input receiver locations that are being integrated over, and $\boldsymbol{x}_{ST}$ is the stationary point associated with this input location. The τ_O isochron is the reflection isochron for the scattered path between the source and the output receiver location. As is described in detail in SB98, the stationary point turns out to be the point where the ray connecting $\boldsymbol{x}_{IG}$ and $\boldsymbol{x}_{OG}$ crosses the $\tau_O = t_O$ isochron. With this location determined, the path lengths r_S, r_{IG}, and r_{OG}, that appear in the integral, are those labeled as such in Figure 1. G is a factor that is a function of the location and derivative along the recording surface, as given in Equation (1), as well as in the Appendix. It is also a function of the stationary point $(\overline{x}_1, \overline{x}_3)$. On a horizontal recording surface, $G = \overline{x}_3$.

Thus, for each input receiver, evaluation of the integral requires knowledge of ray data on a ray path as depicted in Figure 1. A collection of these paths, associated with different input receiver locations is schematically depicted in Figure 2. Note that each ray path has a different stationary point along the isochron. Which of these stationary points represents real reflected energy in the input data depends on the location and shape of the actual subsurface reflectors, and if any of these stationary points represents a specular scattering point along one of them.

Note that since a detailed study of kinematic issues in Kirchhoff datuming already exists in Salinas (1997), using a previously published methodology that is not amplitude preserving, the following discussion will focus primarily on the dynamic calculation, and the ability of the data mapping method to preserve "true" amplitudes, at least in the sense that the amplitude calculation

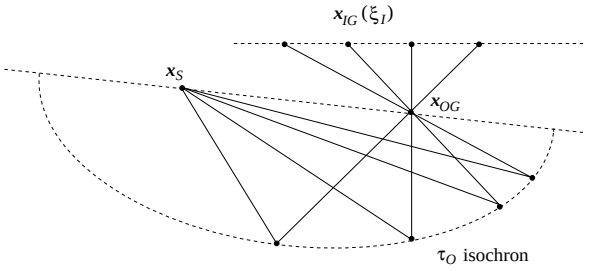

Figure 2. Relevant paths for receiver continuation in a constant wavespeed medium.

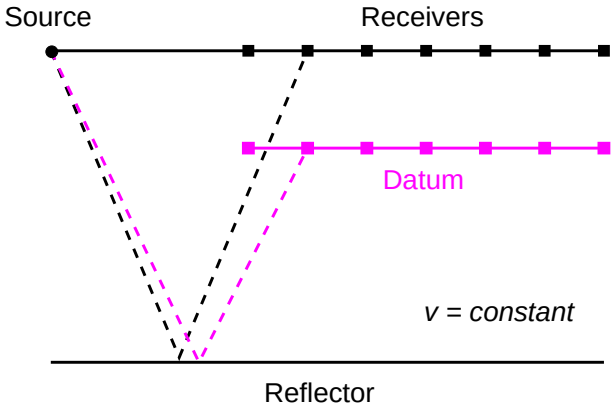

Figure 3. Downward continuation of receivers with horizontal surfaces over a horizontal reflector in constant wavespeed media.

is correct with respect to the wavespeed model that is employed in the downward continuation process.

Horizontal reflector with a horizontal recording surface

The most important features of this method can be illustrated by considering a very basic datuming problem. Given a common source gather, collected on a horizontal recording surface over a single horizontal reflector, consider downward continuation of the receivers to a new horizontal datum. This geometry is depicted in Figure 3.

Data for the tests were generated analytically, by placing a wavelet centered at the proper travel time on each trace, with a peak amplitude defined by 3D geometrical spreading, $1/4\pi r$, where r is the total travel path. The 3D geometrical spreading amplitudes should be accurately mapped in the 2.5D process, so the same procedure is used to generate comparison amplitudes for the datum level.

Consider Figure 4. The first panel shows the input time data for a single, common source gather, collected on a horizontal recording surface over a horizontal reflector at 1500m depth, generated with a 20Hz wavelet. The remaining three panels show the results for downward continuation of the receivers in this gather to horizontal datums at depths of 100m, 500m, and 1000m below the source. These depths are equivalent to roughly 7%, 34%, and 67% of the reflector depth below the source. Kinematically, the calculation is accurate to some maximum offset, beyond which edge effects begin to dominate. It is clear that that amplitudes are anomalously low beyond this limit as well, and the range of accurate data decreases as the datum moves closer to the reflector. Also note the presence of two weak signals which cross above the primary reflection. These are due to effects from the endpoints of integration for the finite aperture data, a topic that is discussed later.

Figure 5 shows plots of amplitudes versus offset for the three downward continued time sections. In each panel, the black curve shows peak amplitudes from the datumed result, whereas the grey curve is an analytic calculation of the peak amplitudes for the desired result. Clearly, they match well over the offsets within a depth-dependent aperture, as indicated in the time sections. At each end of the aperture, the amplitude has a small peak due to the presence of the erroneous arrivals noted above, which constructively interfere with the primary signal at these locations. The range of offsets where the amplitudes are accurate will be referred to as the *useful aperture*.

Note that the size of the useful aperture decreases as the datum is moved closer to the reflector. In cases where the datuming depth is small compared to the depth of the target reflectors, this may not be a large problem. However, in instances where the datum must be evaluated at depths that are significant percentages of the target depth, the range of useful amplitudes may be noticeably restricted. This is an effect of finite aperture data, and is discussed in detail later.

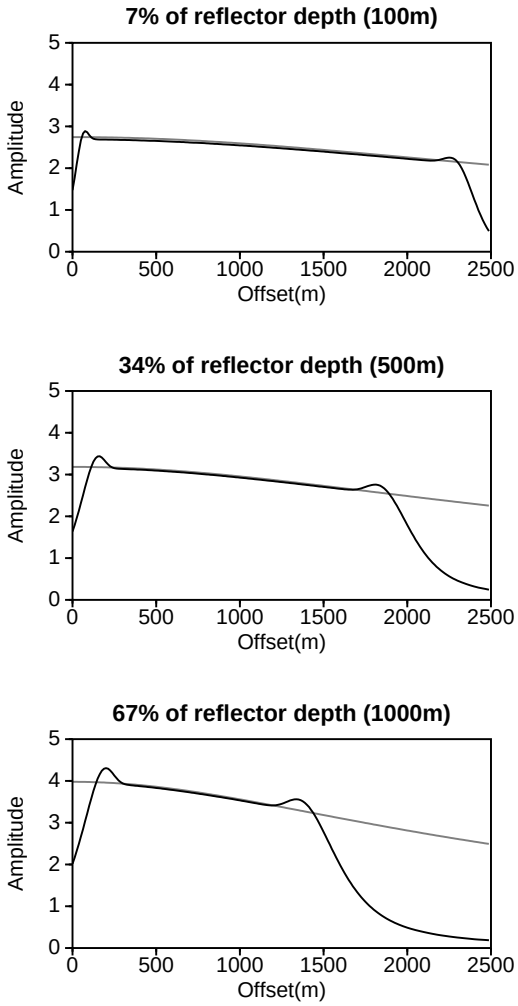

Figure 5. Peak amplitude versus offset for the downward continuation of receivers from a horizontal aquisition surface to three horizontal datum surfaces.

Horizontal reflector with a topographic recording surface

Next, consider the problem depicted in Figure 6. Here a common source survey is carried out over a horizonal reflector, again with a 20Hz wavelet, but with a recording surface that is not horizontal.

In this example, the topography is sinusoidal, with the survey length equal to one topographic wavelength. The amplitude of the surface variation is 250m, over a reflector at 1500m (the figure is not to scale). The receivers are spaced uniformly as measured in the lateral direction, not as measured along the surface. Downward continuation is performed such that the recorded data is transformed to a horizontal output datum, with receiver locations that are, again, spaced evenly in the lateral direction. Here, the lateral spacing is the same as in the input data.

Figure 7 shows the input data containing the effects of the irregular recording surface, and data for downward continued receivers to horizontal datum surfaces at three different depths. Output is shown for Datuming depths of 350m, 500m, and 1000m below the source, corresponding to 28%, 40%, and 80% of the source-reflector depth interval. It can be seen that the kinematic distortion due to the irregular surface has been corrected in the outputs for the horizontal datum surfaces. Again,

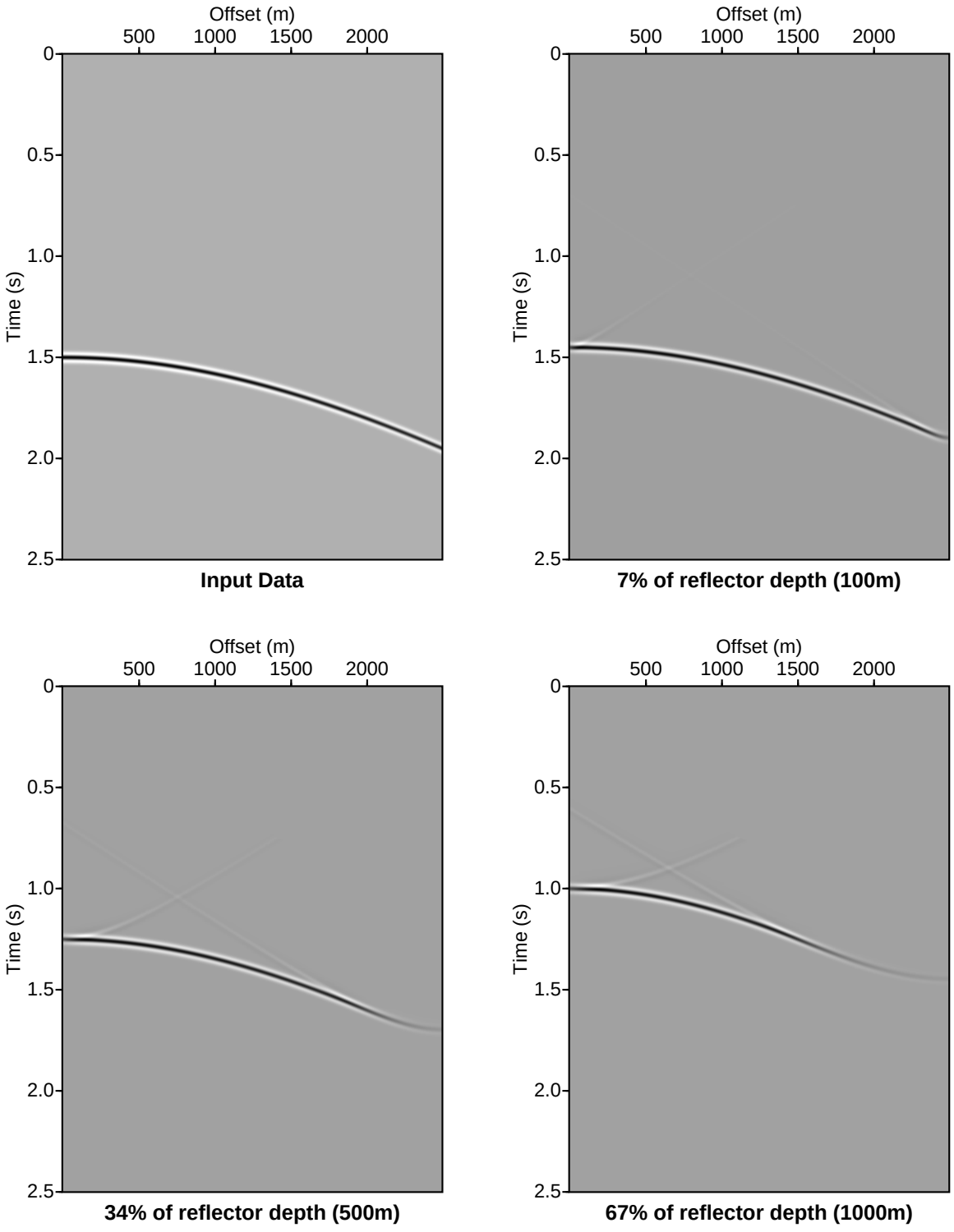

Figure 4. Input and downward continued data for a horizontal reflector and horizontal aquisition and datuming surfaces, showing kinematic results.

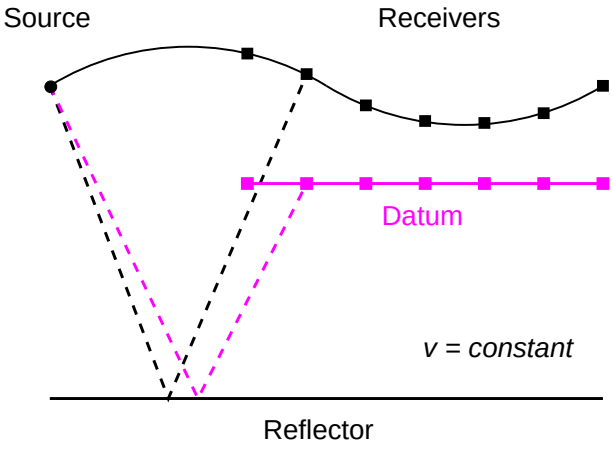

Figure 6. Downward continuation of receivers from a topographic recording surface to a flat datum over a horizontal reflector in constant wavespeed media.

accurate results occur within an aperture that decreases in size as the datum approaches the reflector depth, both for amplitude and kinematics, as in the previous model. As before, two weak erroneous arrivals due to endpoint effects can be seen to join the primary signal at the ends of the aperture.

In Figure 8, the black curve shows peak amplitudes versus offset for the downward continuation of receivers shown in the previous figure. The grey curve is an analytic calculation of the correct peak amplitudes for the desired output, as before. In addition, the dashed grey curve has been added to show the amplitude variation in the original data, displaying the effect of the topographic recording surface on amplitude. This amplitude variation has been corrected in the continued data. As before, amplitudes match well with the analytic prediction within the given aperture, and small amplitude peaks appear at each end of the aperture due to endpoint effects.

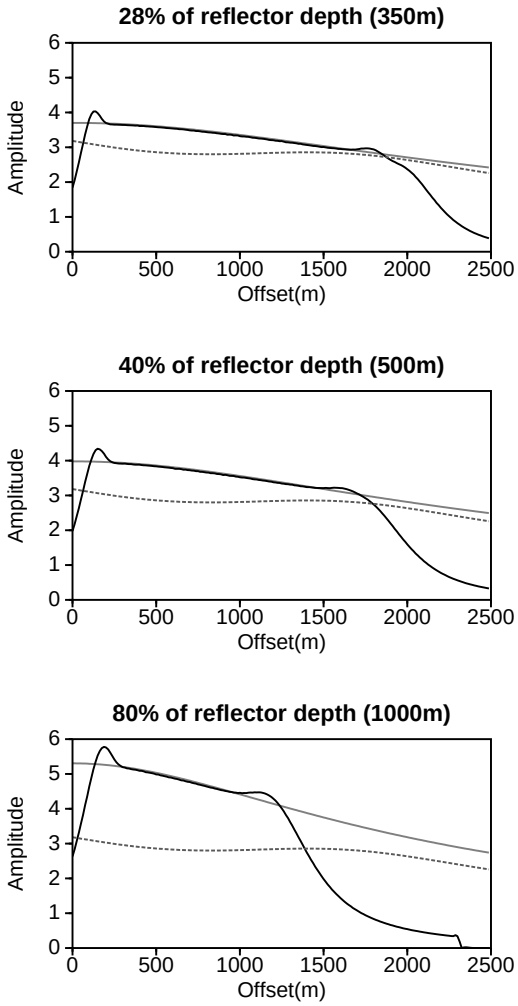

Figure 8. Peak amplitude versus offset for the downward continuation of receivers from a sinusoidal aquisition surface of 250m amplitude to three horizontal datum surfaces.

Irregular reflector with a horizontal recording surface

Next, consider the problem of a horizontal recording surface over a curved reflector. Data is generated using the CSHOT Modeling Program, part of the Center for Wave Phenomena code library at the Colorado School of Mines (Docherty, 1991). This code calculates true amplitude, 2.5D data for reflecting surfaces of irregular shape.

In this example, the recording surface is horizontal, and there is a single, curved reflector, in the shape of an anticline, with an average depth of 1400m, and a relief of 200m. The model and rayapth coverage are depticted in Figure 9. The receivers are spaced uniformly along both the recording and datuming surfaces, with the spacing equal on both the input and output surfaces.

Figure 10 shows the input data containing the effects of the irregular reflecting surface, and the results of the downward continuation of receivers for three different datum surfaces at depths of 300m, 500m, and 800m. These depths correspond to roughly 21%, 36%, and 57% of the average reflector depth below the source. As in the previous examples, the kinematic result is accurate within an aperture that decreases is width as the datum depth appraoaches that of the reflector.

As in the previous amplitude plots, Figure 11 shows peak amplitudes versus offset for the receiver continuation by the black curve. The grey curve shows the amplitudes for the placement of the receivers on the output

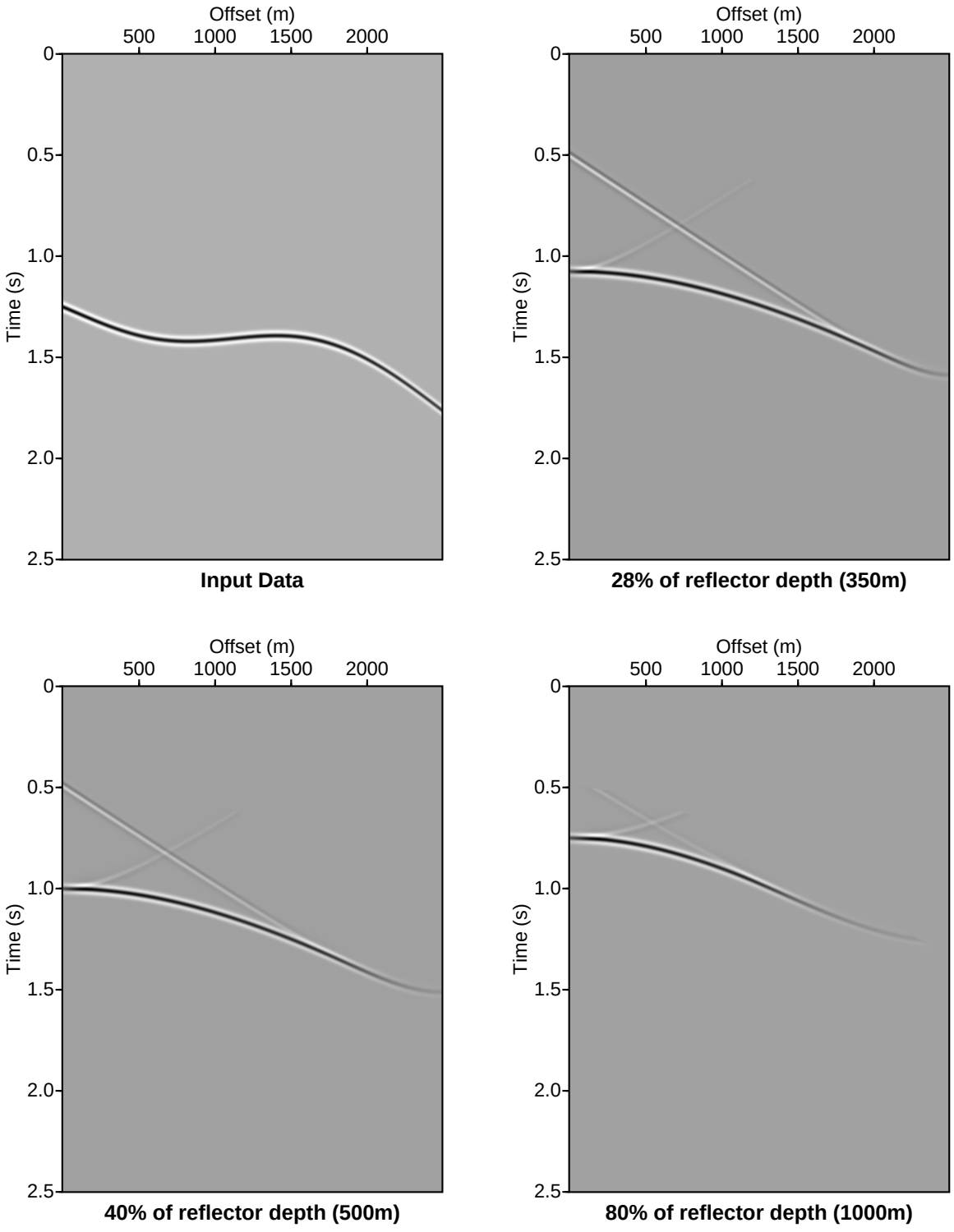

Figure 7. Input and downward continued data for a horizontal reflector and sinusoidal aquisition surface of 250m amplitude, mapped to a horizontal datum at three depths.

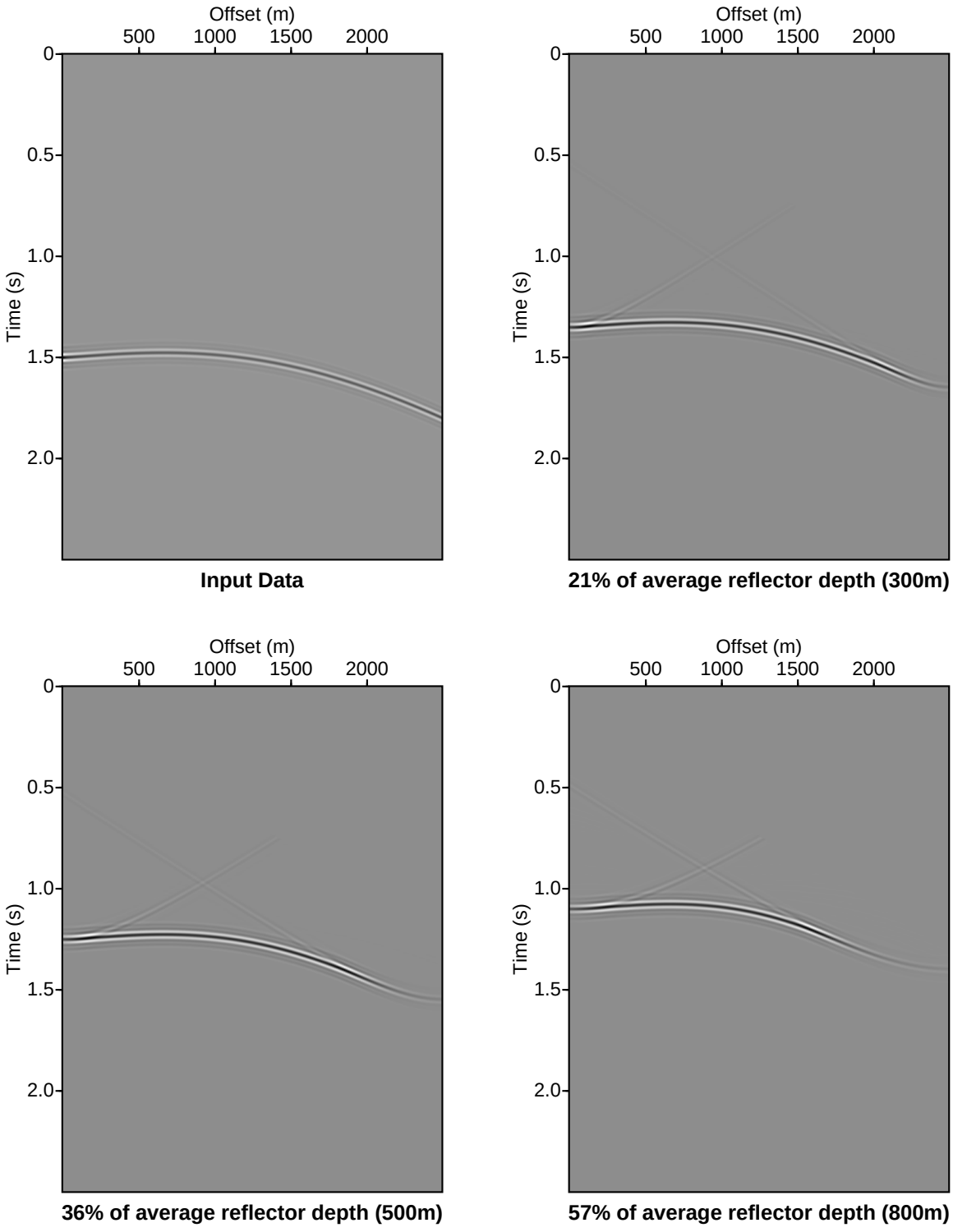

Figure 10. Input and downward continued data for a curved reflector and horizontal aquisition surface, mapped to a horizontal datum at three depths.

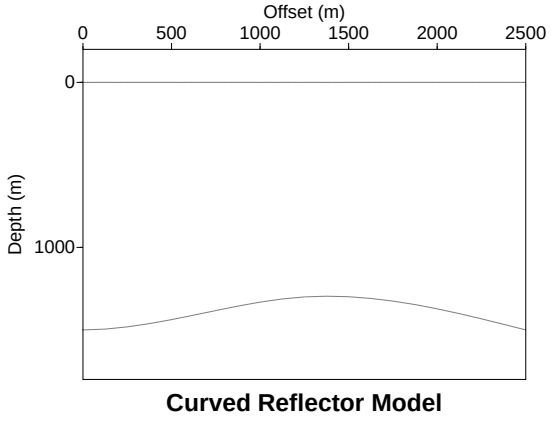

Figure 9. Model for downward continuation of receivers over a curved reflector in constant wavespeed media. The source and receivers are on the zero depth surface.

datum as calculated by the CSHOT modeling code. The dashed grey curve displays the amplitude distribution of the original input data. Again, the amplitudes are correct within a depth dependent useful aperture.

Discussion and Analysis of Results

In this section, both the effects of finite data aperture and the validity conditions for the stationary phase approximations are discussed in terms of the datuming problem. Among other results, it is explained that for a given dominant wavelength in the input data, the stationary phase result is only accurate for characteristic length scales beyond a minimum value. This minimum length scale depends on the curvature of the recording surface, as well as the curvature of traveltime isochrons for rays reaching this surface. Specifically, it is a function of the relative difference between these curvatures.

Finite data aperture

In the datuming examples, it was shown that the method produces accurate amplitudes, but only within a limited range of offsets, previously defined as the useful aperture of the problem. This is an effect of finite aperture data. In practice, data always exists over some finite range of offsets, and this range is not generally large enough for the recorded values of the wavefield go smoothly to zero at the ends of the recording array. This means that amplitudes are only accurate within a useful aperture that is smaller than the finite aperture of the data.

Consider again the integration as depicted in Figure 2. (This figure is drawn for constant wavespeed, but it is simply a schematic that can be generalized to other raypath and isochron shapes.) As previously described, the downward continuation integral is, in practice, a summation over weighted values of a frequency filtered version of the input data, evaluated at the travel time along each of the paths depicted in the figure. In the absence of multipathing, the raypaths imply a one-to-one correspondence between the stationary points along the isochron and each input receiver location, and therefore each data trace. Each stationary point and its associated raypath represents a possible specular reflection in the input data that arrives at the chosen output receiver location at the output time $t_O = \tau_O$. Accurate evaluation of the integral requires that contributions from any of these stationary points associated with real specular reflections

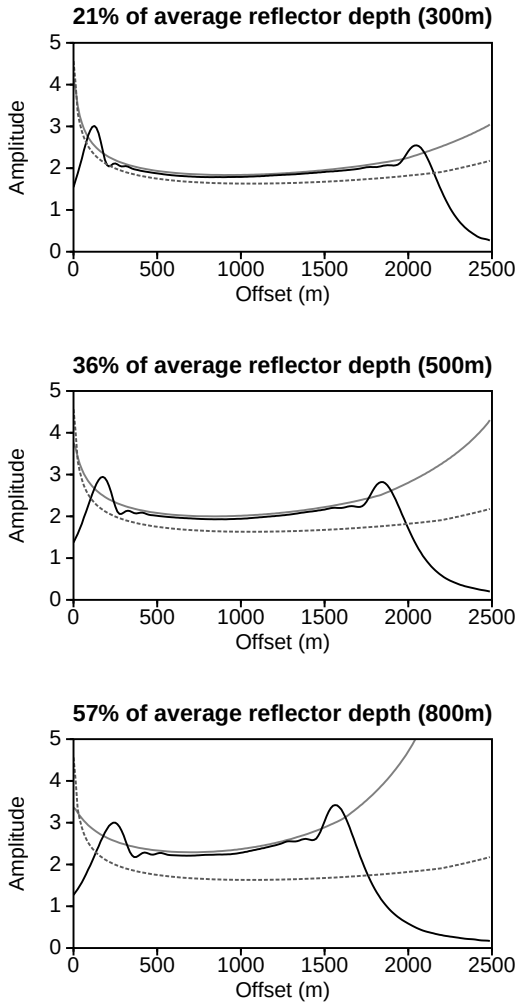

Figure 11. Peak amplitude versus offset for the downward continuation of receivers over a curved reflector to three horizontal datum surfaces.

be included in the summation. However, if these specular rays are associated with recording surface locations that are outside that finite range of the data, then these "missing" values result in an erroneous summation result.

For example, in Figure 2, stationary points on the far left part of the isochron are generally associated with receiver locations on the far right of the recording surface, due to the fixed output location. If some of these far offsets are beyond the maximum offset in the input data, then specular energy associated with these stationary points is not recorded in the input data. If these points are associated with actual specular reflections, then key contributions to the summation are missing, and the resulting wavefield amplitude is not accurate. Similarly, the truncation may occur on the source-side of the survey, as well, for stationary points on the far right part of the isochron that are associated with arrivals at surface locations to the left of the source.

The above discussion considers a single application of the integral, or in other words, the determination of the field at a single output location and time. To define the entire field at all output locations and times requires repeated application of the integral for each point of the output section. Thus, there is some net effect of the data truncation described above for each application of the integral. For a general subsurface model, the regions of the output section for which the field is inaccurate due to these truncations may be diffcult to describe without performing the calculation.

However, for relatively simple, single reflector models, like those shown in this paper, the net effect is simple to describe. In these cases, there is some finite aperture in the output data, inside of which all relevant specular energy is present in the finite input data, and outside of which the specular arrivals are truncated. Hereafter, this is referred to as the *specular aperture*. The specular aperture is a function of the subsurface model, the maximum data offset, and the depth of the output surface.

Consider the specular aperture for the case of a single horizontal reflector, where data is collected out to some maximum offset. Here, there is a single stationary point and raypath associated with the specular reflection from the single reflector to the last data offset. This is depicted in Figure 12. On a datum surface at some depth closer to the reflector, this specular reflection is associated with an output location with a smaller offset. Specular paths associated with locations on the datum directly below the longest offsets in the input data arrive at the recording surface at offsets beyond the last offset in the data. Therefore, the full amplitude of these long offsets is not recovered, since the associated specular reflection is not included in the input data. It should also be clear from the figure that the range of output offsets for which specular data appears in the input data must decrease as the datuming depth approaches that of the reflector. Again, though the specular paths have some other shape in more complicated models, the principle is the same.

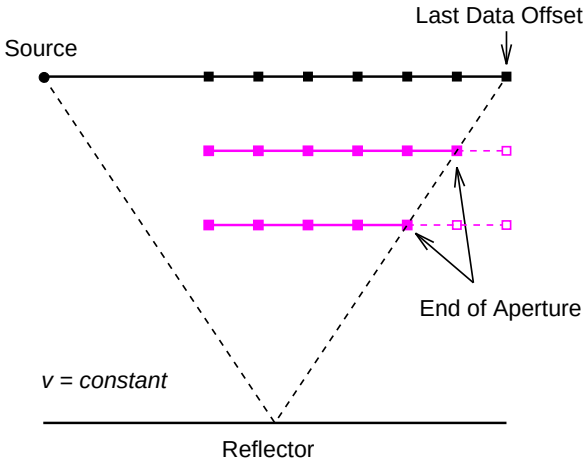

Figure 12. Reduction of useful aperture in the horizontal reflector model.

While the concept of the specular aperture is enough to illustrate that the full amplitude cannot be regained beyond some maximum offset, it does not fully explain the observed amplitudes. For example, the model results of the previous section show that the useful aperture is restricted near zero offset, even in the case of the horizontal reflector where the zero offset specular ray does appear in the data. Furthermore, if the presence or absence of the specular ray were the only aperture limiting mechanism, then the output amplitude would be exactly correct within a specular aperture, and then drop immediately to zero for all offsets beyond that associated with the last specular arrival in the input data. The amplitude function in the model results is clearly more complicated than this, and the useful aperture is generally smaller than the specular aperture for the problem.

A more complete description of these effects of finite data aperture are obtained by examining the phenomena in terms of asymptotics. The method of stationary phase employed in the derivations of the data mapping platform (Bleistein & Jaramillo, 1997, Bleistein, et al. 1998) is the result of a leading order approximation of a more general asymptotic series. This means that the accuracy of the approximation is implicitly dependent upon the assumption that there are no finite endpoints of integration, or at least there are no contributions from such endpoints. These contributions appear in higher order terms that are truncated in the leading order approximation.

Real data is generally finite in extent, so this condition is only satisfied in this case if the data goes smoothly to zero at the endpoints. As previously noted, though, real data does not generally have this property. The result, then, is that amplitudes are inaccurate for any stationary points in the neighborhood of these endpoints, as accuracy of the method relies on the contributions from isolated stationary points bounded well away from any endpoints of integration. For example, Bleistein & Handelsman (1986) show that when a stationary point is coincident with an endpoint of integration, the predicted value is half of the value of an interior stationary point with the same functional value.

The ways in which this pertains to the datuming problem depends on where stationary phase is applied in the derivations, and how the validity of each application is affected by finite data aperture. It turns out that the most important application of stationary phase for this discussion is not that used in the analysis of SB98, but that inherent in the derivation of the data mapping platform itself, from which the results of SB98 are derived.

In Bleistein & Jaramillo (1997), the authors cascade a modeling formula with an inversion formula to derive the so-called data mapping platform, which includes Equation (1) in SB98 for the 2.5D case. Therefore, the validity of the data mapping formula is limited by the conditions on the validity of any asymptotics inherent in either component of the cascade.

As is shown in Bleistein et al. (1998), the inversion formula is derived under the requirement that it produce the correct ray theoretical, "true-amplitude" reflectivity when the input data is Kirchhoff-approximate modeling data for a single reflector of arbitrary shape. This is accomplished, in part, by performing a trial inversion of this Kirchhoff data, and then employing an analysis of the result in the derivation of the final inversion formula. The inversion includes an integration over the recording surface, and in this trial evaluation, the result is obtained by approximating this integral using stationary phase. Thus, data mapping and any processes based upon it, such as the downward continuation of SB98, are only valid under the conditions that this stationary phase approximation of the integration over the recording surface is valid.

This trial inversion involves two spatial integrations. An inner integral over the recording surface, as previosuly noted, and an outer integration over all subsurface depth points, or equaivalently, all potential scattering points. So, when considering the inner integral, there is a fixed source location and fixed scattering point being referenced. Stationary phase picks-out the main energy carrying path between the source, the fixed scattering point, and the recording surface, and assigns a stationary point to the location on the recording surface where this raypath emerges. Whether or not this path represents actual scattered energy in the data depends on the subsurface of the model at hand, so these stationary points and their associated raypaths represent all potential energy carrying paths through all the subsurface points.

Assuming that the input data is of some finite extent, or maximum offset, these stationary points may appear in various neighborhoods of the ends of the finite data aperture. Since the data goes immediately to zero at the ends of the survey, they are effectively endpoints of the surface integration. Thus, contributions from any scattering paths that surface near the ends of the data aperture have incorrect amplitudes. A detailed analysis of this effect is given in Cohen (1990). Of course, in the high frequency limit that is implied by the use of asymptotics, the amplitudes that appear in the output are due primarily to contributions from the subset of stationary points associated with true specular reflections. So, the discussion of the output amplitudes concerns primarily these specular contributions.

In the datuming problem, there is an additional feature, in that the input and output surfaces are different, and this discussion is concerned primarily with the size of the the useful aperture on the output surface. Any raypath in this scheme that surfaces at a stationary point on the input surface is associated with a point, or receiver location, on the output surface. This is, of course, the point where the ray crosses the datum, as previously described by stationarity in the downward continuation. Stationary points associated with true specular raypaths for the subsurface, that are concident with the endpoints of the input data aperture, are associated with the points on the output surface that define the ends of what was previously described as the specular aperture. This was illustrated for a simple case in Figure 12.

So, specular rays associated with stationary points on the input surface that are inside of, but near, the end of the finite data aperture are associated with receiver locations on the output surface that are inside of, but near, the end of the specular aperture in the output data. Since the contributions along these raypaths have erroneous stationary phase amplitudes, due to their proximity to an endpoint of integration on the input surface, then it follows that the output data is inaccurate at the associated offsets on the output surface. Thus, the useful aperture for the downward continued data is generally smaller than the specular aperture, a fact that is evident on the datuming examples presented previously.

All of these finite data aperture effects can be re-

duced or avoided in practice by tapering input data amplitudes so that they go smoothly to zero at the ends. However, while this will generally eliminate the artifacts, it requires the sacrifice of accurate amplitudes in a large number of input traces, and in the end still results in a loss of accuracy a large offsets, and perhaps a smaller useful aperture than would be the case by not tapering. Alternatively, in theory, data could be extended by some synthetic means and allow room for proper tapering. Of course, accurate modeling requires good subsurface models, which may not be available at the time of the application of datuming.

Data mapping and stationary phase

The validity of stationary phase approximations also limits the range of subsurface models for which the datuming process produces correct amplitudes. There is a validity condition that results from the same surface integration as in the finite data aperture discussion, which is a function of the maximum recording surface and reflector curvatures in the problem.

As previously described, Bleistein & Jaramillo (1997) derive equation (1) of SB98 by cascading a modeling formula with an inversion formula, the validity of the result depending on the validity of any asymptotics inherent in each component of the cascade. As dicussed for the case of finite data aperture, this inversion depends on the validity of a stationary phase approximation of an integration over the recording surface. Here, this integration is discussed in more detail.

Consider the following notation. The integration is over the parameter ξ, describing the receiver locations on the recording surface, $\boldsymbol{x}(\xi)$. For the stationary phase approximation of this integral, the shot location is fixed, as is the scattering point, as previously noted. Also, let ϕ be the phase of the reflected wave.

A validity condition for stationary phase in terms of a characteristic length scale L_0, and characteristic frequency ω_0, is derived using dimensionless variables in Bleistein, et al., (1997), as

$$\omega_0 L_0^2 \left| \frac{\partial^2 \phi}{\partial \xi^2} \right| \;\geq\; \pi \,. \tag{4}$$

So, validity for this approximation, as well as data mapping in general, is only ensured when all length scales in the problem obey this condition on L_0. To more easily evalute equation (4), the second derivative of the phase can be defined in terms of other quantities.

First, note that $\phi = \phi(\boldsymbol{x}(\xi))$, with

$$\phi^{'}(\xi) \;=\; \frac{\partial \phi}{\partial x_i}\frac{\partial x_i}{\partial \xi} \;=\; \nabla_{\boldsymbol{x}}\phi \cdot \frac{\partial \boldsymbol{x}}{\partial \xi}\,, \tag{5}$$

and,

$$\begin{aligned} \phi^{''}(\xi) &= \frac{\partial \phi}{\partial x_i}\frac{\partial^2 x_i}{\partial \xi^2} + \frac{\partial x_i}{\partial \xi}\frac{\partial}{\partial \xi}\left(\frac{\partial \phi}{\partial x_i}\right) \\ &= \frac{\partial \phi}{\partial x_i}\frac{\partial^2 x_i}{\partial \xi^2} + \frac{\partial x_i}{\partial \xi}\frac{\partial x_j}{\partial \xi}\frac{\partial^2 \phi}{\partial x_i \partial x_j}\,. \end{aligned} \tag{6}$$

where a summation over the vector components is implied. Consider the above expression to be evaluated at the stationary points, which are those $\boldsymbol{x}(\xi_0)$ satisfying $\phi^{'}(\xi) = 0$. Using equation (5), this stationarity condition is equivalent to

$$\frac{\partial \phi}{\partial \xi} \;=\; \nabla_{\boldsymbol{x}}\phi \cdot \frac{\partial \boldsymbol{x}}{\partial \xi} \;=\; 0\,. \tag{7}$$

Since the derivative of $\boldsymbol{x}$ with respect to ξ is always tangent to the recording surface, this condition implies that stationarity occurs at points $\boldsymbol{x}(\xi_0)$ where $\nabla_{\boldsymbol{x}}\phi$ is normal to this surface.

The actual form of the parameter ξ is unspecified, so relate it to a parameter s denoting arclength along the recording surface. Then,

$$\frac{\partial \boldsymbol{x}}{\partial s} \;=\; \frac{\partial \boldsymbol{x}}{\partial \xi}\frac{\partial \xi}{\partial s}\,, \tag{8}$$

$$\frac{\partial^2 \boldsymbol{x}}{\partial s^2} \;=\; \frac{\partial^2 \boldsymbol{x}}{\partial \xi^2}\left(\frac{\partial \xi}{\partial s}\right)^2 \;+\; \frac{\partial \boldsymbol{x}}{\partial s}\frac{\partial^2 \xi}{\partial s^2}\,. \tag{9}$$

Let $\hat{\boldsymbol{n}}$ be a vector normal to the recording surface, and dot this normal into both sides of equation (9) to give

$$\hat{\boldsymbol{n}} \cdot \frac{\partial^2 \boldsymbol{x}}{\partial s^2} \;=\; \hat{\boldsymbol{n}} \cdot \frac{\partial^2 \boldsymbol{x}}{\partial \xi^2}\left(\frac{\partial \xi}{\partial s}\right)^2\,, \tag{10}$$

where the second term vanishes because the derivative of $\boldsymbol{x}$ with respect to arclength is always tangent to the surface. Note also that, at stationarity,

$$\frac{\partial \phi}{\partial \boldsymbol{x}} \;=\; \pm\,|\nabla_{\boldsymbol{x}}\phi|\;\hat{\boldsymbol{n}}\,. \tag{11}$$

So, if both sides of equation (10) are multiplied by the magnitude of the gradient of the phase, equation (11) allows the result to be written in summation form as,

$$\frac{\partial \phi}{\partial x_i}\frac{\partial^2 x_i}{\partial \xi^2} \;=\; \pm\,|\nabla_{\boldsymbol{x}}\phi|\left(\frac{\partial s}{\partial \xi}\right)^2 \hat{n}_i \frac{\partial^2 x_i}{\partial s^2}\,. \tag{12}$$

Now, consider the traveltime isochron passing through each of the stationary points. This isochron is associated with travel along a raypath, though a fixed depth point, that surfaces at the stationary point, as previously described by the stationarity condition on the ξ integral. Since the isochron is associated with a particular stationary point, it can be considered a function of ξ.

Further, let the arclength along the isochron is denoted by the parameter γ, and the points along the isochron by $\boldsymbol{y}(\gamma)$. Conisdering the fact that an isochron is a surface of constant phase, these parameters allow the isochron to be defined as

$$\phi\left(\boldsymbol{y}(\gamma),\xi\right) \;=\; C(\xi)\,, \tag{13}$$

where $C(\xi)$ is a constant along the isochron. Thus,

$$\phi^{'}\left(\gamma\right) \;=\; \frac{\partial\phi}{\partial y_i}\,\frac{\partial y_i}{\partial\gamma} \;=\; 0\,, \tag{14}$$

at all points along the isochron. Since γ is a parameter along the isochron, equations (13) and (14) imply that the second derivative is also zero at all points on the isochron. Thus,

$$\begin{aligned}\phi^{''}(\gamma) \;&=\; \frac{\partial\phi}{\partial y_i}\,\frac{\partial^2 y_i}{\partial\gamma^2} + \frac{\partial y_i}{\partial\gamma}\,\frac{\partial}{\partial\gamma}\left(\frac{\partial\phi}{\partial y_i}\right)\\ &=\; \frac{\partial\phi}{\partial y_i}\,\frac{\partial^2 y_i}{\partial\gamma^2} + \frac{\partial y_i}{\partial\gamma}\,\frac{\partial y_j}{\partial\gamma}\,\frac{\partial^2\phi}{\partial y_i\partial y_j} \;=\; 0\,.\end{aligned} \tag{15}$$

The isochron and the recording surface share a single common point, the stationary point, where $\boldsymbol{y}=\boldsymbol{x}$. The gradient of the phase, $|\nabla_{\boldsymbol{x}}\phi|$, is always normal to the isochron, by definition. At a stationary point, the required condition is that this gradient be colinear with the normal to the recording surface. Thus, the isochron is tangent to the recording surface there. In this case, then, at each stationary point,

$$\frac{\partial y_i}{\partial\gamma} \;=\; \frac{\partial x_i}{\partial s} \;=\; \frac{\partial x_i}{\partial\xi}\left(\frac{\partial\xi}{\partial s}\right)\,. \tag{16}$$

Using this result and letting $\boldsymbol{y}=\boldsymbol{x}$, the second derivative expression in equation (15) can be rewritten as,

$$\frac{\partial\phi}{\partial x_i}\,\frac{\partial^2 x_i}{\partial\gamma^2} + \frac{\partial x_i}{\partial\xi}\,\frac{\partial x_j}{\partial\xi}\left(\frac{\partial\xi}{\partial s}\right)^2\frac{\partial^2\phi}{\partial x_i\partial x_j} \;=\; 0\,, \tag{17}$$

or equivalently, using equation (11),

$$\frac{\partial x_i}{\partial\xi}\,\frac{\partial x_j}{\partial\xi}\,\frac{\partial^2\phi}{\partial x_i\partial x_j} \;=\; \mp|\nabla_{\boldsymbol{x}}\phi|\left(\frac{\partial s}{\partial\xi}\right)^2\hat{n}_i\frac{\partial^2 x_i}{\partial\gamma^2}\,, \tag{18}$$

at each stationary point.

Finally, then, the second derivative expression at each stationary point given in equation (6) can be rewritten using equation (12) to rewrite the first term, and equation (18) to redefine the second term, giving,

$$\phi^{''}\left(\xi\right) \;=$$

$$|\nabla_{\boldsymbol{x}}\phi|\left(\frac{\partial s}{\partial\xi}\right)^2\left[\pm\hat{n}_i\frac{\partial^2 x_i}{\partial s^2} \;\mp\; \hat{n}_i\frac{\partial^2 x_i}{\partial\gamma^2}\right]\,. \tag{19}$$

The two terms in the brackets have undetermined but opposite sign, owing to the use of equation (11) in the determination of the right sides of equations (12) and (18). Thus, combining the signs in front of the equation, and collapsing the summations to vector form, gives,

$$\phi^{''}\left(\xi\right) \;=$$

$$\pm\,|\nabla_{\boldsymbol{x}}\phi|\left(\frac{\partial s}{\partial\xi}\right)^2\left[\hat{\boldsymbol{n}}\cdot\frac{\partial^2\boldsymbol{x}}{\partial s^2} \;-\; \hat{\boldsymbol{n}}\cdot\frac{\partial^2\boldsymbol{x}}{\partial\gamma^2}\right]\,. \tag{20}$$

Substituting the absolute value of this derivative into equation (4) yields a validity condition,

$$\omega_O L_O^2\,|\nabla_{\boldsymbol{x}}\phi|\left(\frac{\partial s}{\partial\xi}\right)^2\left|\hat{\boldsymbol{n}}\cdot\frac{\partial^2\boldsymbol{x}}{\partial s^2} \;-\; \hat{\boldsymbol{n}}\cdot\frac{\partial^2\boldsymbol{x}}{\partial\gamma^2}\right| \;\geq\; \pi \tag{21}$$

The dot products with the surface normal are the magnitudes of the curvature of the recording surface, κ_ξ, and the curvature of the isochron, κ_ϕ, at this stationary point. So, the validity condition is equivalently,

$$\omega_O L_O^2\,|\nabla_{\boldsymbol{x}}\phi|\left(\frac{\partial s}{\partial\xi}\right)^2|\kappa_\xi-\kappa_\phi| \;\geq\; \pi \tag{22}$$

Remember that this result determines the validity of the approximation at a particular stationary point. So, for a given a characteristic frequency and length scale, the above restriction on the realtive curvatures of the recording surface and isochron must be applied at *every* stationary point to ensure that the overall output is accurate. In practice, since only stationary points corresponding to real specular reflections contribute significantly to the output amplitudes, this condition can be relaxed slightly, to require that this relationship hold at all stationary points associated with the arrival of specular energy. Typically, though, which points these are is not known at the time of the application of the data mapping process, so, in practice, it is best to require that that the maximum recording surface and isochron curvatures for the entire domain not violate this condition.

While the maximum recording surface curvature is easily observed, the maximum isochron curvature at the surface is not. So, in practice, this quantity must be estimated using whatever *a priori* information about the wavespeed profile and target depths is available to produce a "worst case" isochron curvature at the surface.

Comparison with Conventional Datuming Methods

In this section, methodology and results are compared with a conventional Kirchhoff wave-equation-datuming

method in constant wavespeed reference media. By this, reference is being made specifically to the method of Berryhill (1979, 1984), as it is specialized to 2.5D in Bevc (1995) and in Salinas (1997).

Comparison of this method with the data mapping results shows that while the two are identical kinematically, they have significant differences in the dynamic part of the calculation. Therefore, the conventional method does not yield true-amplitudes for 2.5D, even in constant wavespeed media.

Analytic comparisons

All references here to the *conventional Kirchhoff method* for wave equation datuming, are to the method by which Green's theorem is applied over a hemispherical volume, thus allowing the use of the method of images to eliminate the derivative of the field from the integrand. Consequently, the geometry explicitly assumes a horizontal aquisition surface. This result is given for a single wavefield in a constant wavespeed medium in 3D by Berryhill (1979, 1984). This integral expression is specialized to 2.5D by Bevc (1995) and by Salinas (1997), via an integration over the out-of-plane variable using stationary phase, and making the far-field approximation. The expression for downward continuation given by Bevc (1995), in his variables, is

$$P(\boldsymbol{r},\omega) \;\approx\; \frac{1}{\sqrt{2\pi c}} \int \frac{1}{\sqrt{r}} \frac{\partial r}{\partial n} \sqrt{i\,\omega}\; P(\boldsymbol{r}_S,\omega)\, e^{-i\omega r/c}\; dx \;, \qquad (23)$$

where r s the distance between the output location being evaluated and the recording surface at each input receiver location. The integration is over the linear survey, and is parameterized by x.

In order to make a direct comparison of this result to the data mapping results in this paper, it is necessary to write the conventional expression in terms of the variables used in this paper. Note that if the horizontal recording surface is at $z = 0$,

$$r \;=\; r_{IG} - r_{OG}, \qquad \frac{\partial r}{\partial n} = \cos\theta = \frac{\overline{x}_3}{r_{IG}} \;, \qquad (24)$$

noting that the $\cos\theta$ refers to the definition of the emergence angle in Bevc(1995), and not the ray opening angle as defined in SB98. These equations allow (23) to be written as

$$U_O(\xi_O,\omega) \;\approx\; \frac{1}{\sqrt{2\pi c}} \cdot \int \frac{\overline{x}_3}{r_{IG}} \frac{\sqrt{i\,\omega}\; u_I(\xi_I,\omega)}{\sqrt{|r_{IG}-r_{OG}|}}\; e^{-i\omega(r_{IG}-r_{OG})/c}\; d\xi_I. \quad (25)$$

Here, the upper case U_O indicates that the result is from this conventional method. We have also assumed the case of downward continuation of receivers. Rewriting the phase in terms of constant wavespeed travel times produces,

$$U_O(\xi_O,\omega) \;\approx\; \frac{1}{\sqrt{2\pi c}} \cdot \int \frac{\overline{x}_3}{r_{IG}} \frac{\sqrt{i\,\omega}\; u_I(\xi_I,\omega)}{\sqrt{|r_{IG}-r_{OG}|}} e^{-i\omega t_I}\; e^{i\omega t_O}\; d\xi_I \;. \qquad (26)$$

where t_I and t_O represent the constant velocity travel times for the input and output receiver locations, respectively. Now, perform the inverse Fourier transform from ω to t_O, yielding

$$U_O(\xi_O,t_O) \;\approx\; \frac{1}{\sqrt{2\pi c}} \cdot \frac{1}{2\pi} \iint \frac{\overline{x}_3}{r_{IG}}\; \frac{\sqrt{i\,\omega}\; u_I(\xi_I,\omega)}{\sqrt{|r_{IG}-r_{OG}|}}\; e^{-i\omega t_I}\; d\omega\; d\xi_I \;. \quad (27)$$

For the sake of comparison, write this in more compact form, as

$$U_O(\xi_O,t_O) \;\approx\; \iint F(\xi_O,t_O)\, d\omega\; d\xi_I \;. \qquad (28)$$

Direct comparison of Equation (27) with the analogous data mapping result for a horizontal recording surface, Equation (3) with $G = \overline{x}_3$, allows the latter to be defined in terms of the integrand in Equation (28) as

$$u_O(\xi_O,t_O) \;=\; \iint \frac{\sqrt{r_S + r_{IG}}}{\sqrt{r_S + r_{OG}}}\, F(\xi_O,t_O)\; d\omega\; d\xi_I \;. \quad (29)$$

This expression illustrates that the conventional method is identical to the data mapping result in terms of kinematics, but does not contain all of the factors necessary to correctly calculate amplitudes. The amplitude weights in the integrand differ by a function of the path lengths to and from the given stationary point, which 2.5D theory identifies as exactly the out-of-plane geometrical spreading correction. The influence of this factor is clearly greater when the datuming depth approaches that of the reflector, all other things being equal.

The Green's function approach used to derive the conventional result has the limitation that it explicity requires that the recording surface be flat. In the presence of an irregular recording surface, a commonly used

modification is to assume that the surface curvatures are small, and use the flat surface form of the integral with the correct path lengths (Salinas, 1997). Therefore, the effects of the topography are only addressed via these modified path lengths, and a locally horizontal surface is implicitly assumed at every receiver location. While considering the path lengths correctly will handle the kinematics appropriately, the assumption of a locally flat surface will introduce an additional dynamic error, since the amplitude weights depend on derivatives of the function defining the data surface, as is shown in the data mapping results.

So, in the case of a general recording surface, and using these assumptions, the direct comparison of (27) with the data mapping result for a general surface (3) adds a factor such that equation (29) can be generalized to

$$u_O\left(\xi_O, t_O\right) \; = \; \iint \frac{G\left(\overline{x}_1, \overline{x}_3\right)}{\overline{x}_3} \frac{\sqrt{r_S + r_{IG}}}{\sqrt{r_S + r_{OG}}} F\left(\xi_O, t_O\right) \, d\omega \; d\xi_I \; , \quad (30)$$

in the topographic case.

Note that the conventional result requires only the path lengths r, connecting points on the recording surface with points on the datum, and the travel times along them. Both of the additional amplitude factors associated with the data mapping result, however, require path lengths connecting both the datum and recording surfaces with stationary points that lie well below the datum.

This result is specifically derived here for homogenous media, however, this implication can be extended to the general inhomogenous case, as well. The previous derivations in this paper show that in inhomogenous media, the data mapping result has more complicated amplitude factors than the constant wavespeed case, but the form of the path dependent factors is roughly the same, with the substitution of parameters σ_{IG}, σ_{OG}, and σ_S for r_{IG}, r_{OG}, and r_S, where these parameters are defined by $d\sigma = c^2 d\tau$ along the respective raypath. The inhomogenous form of the conventional expression is not derived here, but one can surmise from the approach, at least heuristically, that the amplitude weights will depend on quantities associated with the paths between the datum and recording surface only, analogous to the homogenous case. *So, in general, the conventional Kirchhoff approach only requires a knowledge of the subsurface between the recording surface and the datum, but the data mapping result shows that a knowledge of the subsurface to depths well below that of the datum is required to accurately calculate amplitudes, using Kirchhoff-like methods, at least in the 2.5D case.*

Comparison of synthetic results

To examine the effects of the "missing" factors in the integrand of the conventional Kirchhoff datuming expression, amplitude results for the data mapping approach are shown in direct comparison to those resulting from the conventional approach. As previously noted, the kinematic results of the two methods are identical, so our comparison focuses on the preservation of amplitude.

Figures (13), (14), and (15) show peak amplitudes versus offsets for the three datuming examples, for downward continuation of receivers to horizontal datums. As before, the grey curve is an analytic calculation of the proper output amplitude function, and the black curve the data mapping result. However, now the dashed curve is the result of performing the same downward continuation using the conventional Kirchhoff datuming approach given by equation (27). In the conventional calculation of the topographic recording surfaces, the topography is accounted for by using the correct path lengths in the standard integral, as previously discussed.

First, a model with a horizontal reflector and a horizontal recording surface, identical to that presented earlier, is considered. Figure (13) shows that the data mapping method is yielding correct amplitudes within a particular aperture. The conventional amplitudes appear to be a good approximation for the shallow datum, where the function of path lengths in equation (29) is near unity. As the datum is moved closer to the reflector, though, the conventional amplitudes are increasingly too low, but they appear to have roughly correct relative values with respect to offset. This last result, however, is only a by-product of the simple geometry of the problem, since the amplitude factor missing from the conventional result is not, in general, nearly constant, as is evidenced by equation (29).

Next, consider two models with a horizontal reflector and a sinusoidal recording surface. When the aquisition surface is not horizontal, the integrands differ by an additional factor, as evidenced in equation (30), which is not necessarily close to unity when the datuming depth is small compared to the reflector depth, and is dependent on the topography of the surface. This is clear in Figure (14), where the recording surface is a sinusoid of 125m amplitude, and in Figure (15), where the recording surface is a sinusoid of 250m amplitude. In both cases, the conventional result is incorrect in absolute and relative amplitude, even for this simple topography. From these results, it's clear that the error increases as the variations along the recording surface increase in dip.

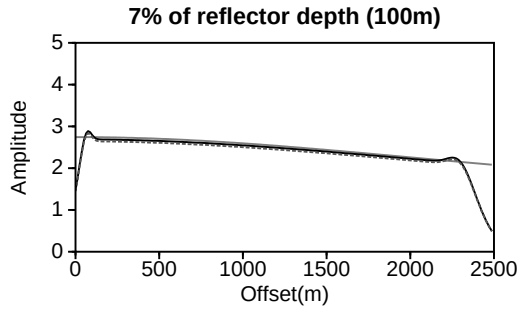

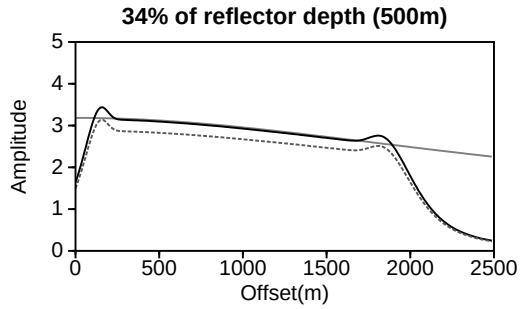

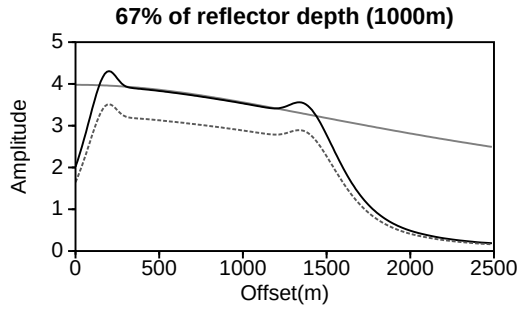

Figure 13. Comparison of peak amplitudes for data mapping and conventional datuming of receivers from a horizontal aquisition surface.

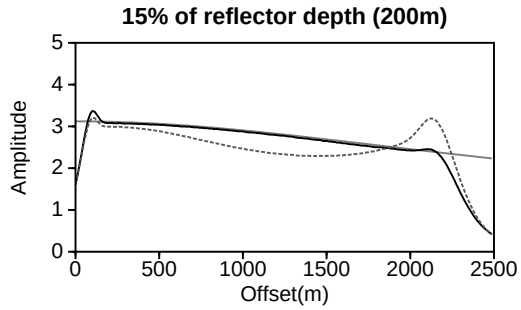

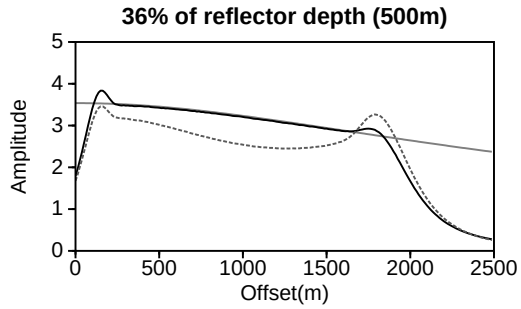

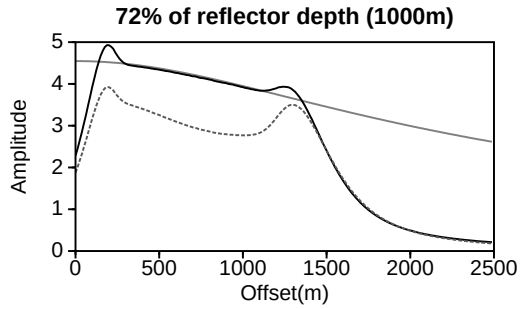

Figure 14. Comparison of peak amplitudes for data mapping and conventional datuming of receivers from a sinusoidal aquisition surface of 125m amplitude.

Indeed, the error increases as the surface variations become larger or more frequent. The same holds true for downward continuation in any wavespeed model. So, for purposes of amplitude preservation, conventional Kirchhoff datuming methods are not strictly correct, even in simple, homogenous models, except those with shallow datuming depths and flat aquisition surfaces.

Discussion

A careful caveat is included in the statement that true-amplitude Kirchhoff datuming requires evaluations of quantities along raypaths to locations below the datum, thus requiring a knowledge of much more of the subsurface than just that between the datum and the recording surface. This statement pertains only to *Kirchhoff-based* methods. Techniques such as phase-shift extrapolation and finite difference approximations only require evaluations within the part of the medium through which the wavefield is being extrapolated, here between the datum and the recording surface. This makes sense physically, since these are direct evaluations of the wave equation. It is clear, even intuitively, that the medium outside of the propagation/depropagation region will not influence the result.

However, Kirchhoff methods are most accurately described as *representations* of the wave propagation problem, through the use of of Green's Theorem, where integrations are performed over a representative wavefield on some boundary surface, a part of which is usually a

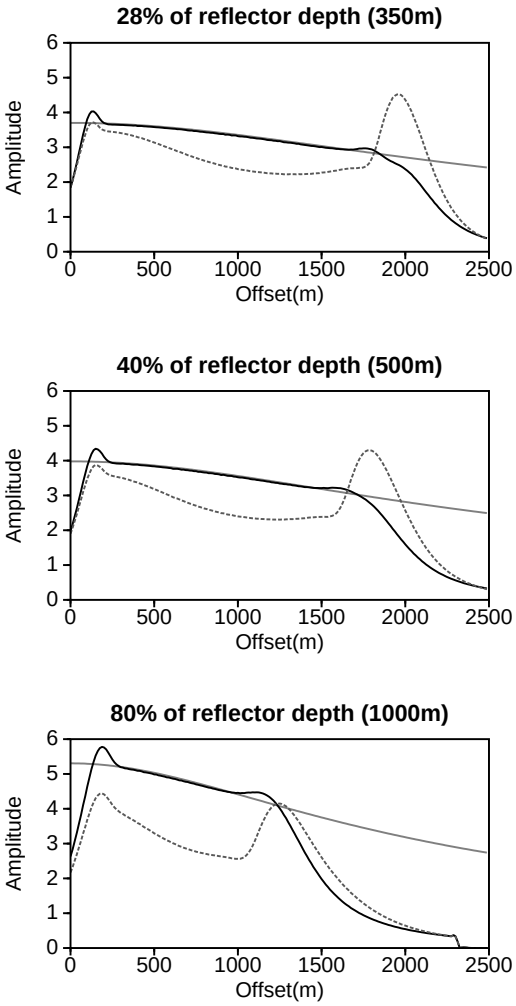

Figure 15. Comparison of peak amplitudes for data mapping and conventional datuming of receivers from a sinusoidal aquisition surface of 250m amplitude.

hemisphere with a radius that is allowed to increase towards infinity. This surface integration is a construction, and, in the case of reverse propagation where the surface integral over the hemisphere is not zero, the Kirchhoff representation is not an exact solution to the wave equation. So, the Kirchhoff construction cannot necessarily be intuitively interpreted in exactly the same way as the direct propagation methods.

The approach used in Berryhill (1979), Bevc (1995), and Salinas (1997) assumes Green's Theorem on a hemispherical bounding surface, and employs the method of images so that only one field quantity is required to evaluate the surface integral. (See the references for details.) For forward propagation, the integral over the curved part of the boundary is assumed to go to zero as the radius of the hemisphere becomes infinite. This leaves the flat upper surface of the hemisphere as the only contributing part of the surface integral, which is perfectly applicable to input data collected at the Earth's, or other, horizontal surface. In this result, only the paths between the datum and the horizontal data surface need to be evaluated.

If the same approach is attempted for reverse propagation, however, it is problematic to assume that any part of the bounding surface can ignored, even when the size of the volume becomes infinite. Diffuse energy on the boundary must focus to scattering sources in the volume. The problem encountered is what the appropriate contribution of this surface should be, especially in 2.5D. There is little phyiscal insight in this conventional construction that can elucidate this, so it is generally ignored, as in the forward propagating case. Since the data mapping result does not use this type of construction in any way, comparison of the results in this study with the conventional method suggest that the contribution of this surface in the 2.5D problem is exactly the out-of-plane spreading factor that is missing from the conventional result. Further, it implies that the evaluation of ray data at stationary points below the datum is analogous to including an integration over this surface. However, no more rigorous or physical evidence for why this should be the case is provided here, and the conclusion is drawn only from direct comparison of the two results and the assumptions implicit in them.

References

J.R. Berryhill, 1979, *Wave-equation Datuming.* Geophysics, 44, 1329-1344.

J.R. Berryhill, 1984, *Wave-equation Datuming Before Stack (Short Note).* Geophysics, 49, 2064-2066.

D. Bevc, 1995, *Imaging Under Rugged Topography and Complex Velocity Structure.* Ph.D. Thesis, Stanford University.

N. Bleistein & H. Jaramillo, 1997, *A Platform for Data Mapping in Scalar Models and Data Aquisition.* CWP-267, Colorado School of Mines.

N. Bleistein, J.K. Cohen, J. Stockwell, Jr., 1998, *Mathematics of Multidimensional Seismic Inversion.* Course notes, Colorado School of Mines, in preparation.

N. Bleistein, 1998, *2.5D Data Mappings.* In preparation.

N. Bleistein, 198?, *Mathematical Methods for Wave Phenomena.* Academic Press, New York.

N. Bleistein & R.A. Handelsman, 1986, *Asymptotic Expansions of Integrals.* Dover Publications, New York.

J.K. Cohen, 1990, *Aperture for Kirchhoff Inversion.* CWP-079R, Colorado School of Mines.

P. Docherty, 1991, *Documentation for the 2.5D Common-Shot Modeling Program CSHOT.* CWP-U08R, Colorado School of Mines.

T. Salinas, 1997, *The Influence of Near-Surface Time Anomalies in the Imaging Process.* M.Sc. Thesis, Colorado School of Mines.

S. Sheaffer & N. Bleistein, 1998, *2.5D Downward Continuation Using Data Mapping Theory.* CWP Annual Project Review, CWP-283.

APPENDIX A: Corrected derivation of the factor G for constant-wavespeed media

This appendix contains the corrected derivation of the topographic factor $G(\overline{x}_1, \overline{x}_3)$, superceding the erroneous Appendix in Sheaffer & Bleistein (1998), in the 1998 CWP Project Review. The results of this derivation replace the results given in equations (36) and (61) of that paper.

Here, consider receiver continuation, and let the source and receiver locations be defined as in Sheaffer & Bleistein (1998), that is,

$$\begin{aligned} \boldsymbol{x}_{IG} &= (\xi_I, z_I(\xi_I)) \ , \qquad \boldsymbol{x}_{OG} = (\xi_O, z_O) \ , \\ \boldsymbol{x}_S &= (x_S, z_S(\xi_I)) \ , \end{aligned} \tag{A1}$$

and the stationary point is denoted by,

$$\boldsymbol{x} = (\overline{x}_1, \overline{x}_3) \ . \tag{A2}$$

The path r_{IG} is represented by the vector

$$\boldsymbol{r}_{IG} = ((\overline{x}_1 - \xi_I), (\overline{x}_3 - z_I)) \ . \tag{A3}$$

The gradient of the isochron associated with waves propagating along this path is a vector pointing in the direction of $\boldsymbol{r}_{IG}$ with magnitude $1/c$, or

$$\nabla_{\boldsymbol{x}} \tau_{IG} \ = \ \frac{\boldsymbol{r}_{IG}}{c\, r_{IG}} \ = \ \frac{1}{c\, r_{IG}} \left((\overline{x}_1 - \xi_I), (\overline{x}_3 - z_I)\right) \ . \tag{A4}$$

The derivative of this gradient with respect to the parameter ξ_I is then

$$\frac{\partial \nabla_{\boldsymbol{x}} \tau_{IG}}{\partial \xi_I} \ = \ \frac{\partial}{\partial \xi_I} \left(\frac{\overline{x}_1 - \xi_I}{c\, r_{IG}} \right) \hat{x}_1 + \frac{\partial}{\partial \xi_I} \left(\frac{\overline{x}_3 - z_I}{c\, r_{IG}} \right) \hat{x}_3 \ , \tag{A5}$$

where $\hat{x}_1$ and $\hat{x}_3$ are unit vectors along the corresponding coordinate axes. Remembering that z_I is a function of ξ_I, performing the differentiations on the right side in more detail, yields,

$$\begin{aligned} &\frac{\partial \nabla_{\boldsymbol{x}} \tau_{IG}}{\partial \xi_I} \ = \\ &\frac{1}{c\, {r_{IG}}^3} \left[(\overline{x}_1 - \xi_I)(\overline{x}_3 - z_I) \frac{\partial z_I}{\partial \xi_I} - (\overline{x}_3 - z_I)^2 \right] \hat{x}_1 \\ &+ \frac{1}{c\, {r_{IG}}^3} \left[(\overline{x}_1 - \xi_I)(\overline{x}_3 - z_I) - (\overline{x}_3 - z_I)^2 \frac{\partial z_I}{\partial \xi_I} \right] \hat{x}_3 \ . \end{aligned} \tag{A6}$$

Calculating the magnitude of the vector produces a perfect square in terms of the derivative, yielding,

$$\left| \frac{\partial \nabla_{\boldsymbol{x}} \tau_{IG}}{\partial \xi_I} \right| \ = \ \frac{1}{c\, {r_{IG}}^2} \left| (\overline{x}_3 - z_I) - (\overline{x}_1 - \xi_I) \frac{\partial z_I}{\partial \xi_I} \right| \ . \tag{A7}$$

In the text, the second factor is expressed as G, so that

$$\left| \frac{\partial \nabla_{\boldsymbol{x}} \tau_{IG}}{\partial \xi_I} \right| = \frac{G(\overline{x}_1, \overline{x}_3)}{c\, {r_{IG}}^2} \ , \tag{A8}$$

where this G replaces that given in SB98.

The expression for this factor for source continuation follows an analogous derivation, where only the source and receiver parameters are interchanged.